THE JOURNAL OF BIOLOGICAL CHEMISTRY VOL. 290, NO. 27, pp. 16894–16905, July 3, 2015

Human SLC4A11 Is a Novel NH_3/H^+ Co-transporter*

Received for publication, November 30, 2014, and in revised form, May 26, 2015 Published, JBC Papers in Press, May 27, 2015, DOI 10.1074/jbc.M114.627455

Wenlin Zhang[‡], **Diego G. Ogando**[‡], **Joseph A. Bonanno**[‡1], **and Alexander G. Obukhov**[§2]

From the [‡]*School of Optometry, Indiana University Bloomington, Bloomington, Indiana 47405 and the* [§]*Department of Cellular and Integrative Physiology, Indiana University School of Medicine, Indianapolis, Indiana 46202*

Background: Mutations in SLC4A11 result in corneal endothelial dystrophies; however, the transport characteristics of this membrane protein remain unclear.
Results: SLC4A11 showed NH_4Cl-dependent currents indicative of a NH_3/H^+ electrogenic co-transport mode.
Conclusion: SLC4A11 is a novel NH_3/H^+ co-transporter, uncharacteristic of the SLC4 bicarbonate transporter family.
Significance: SLC4A11 ammonia transport capacity should be considered along with other NH_3 transporters/channels when examining tissue nitrogen homeostasis.

SLC4A11 has been proposed to be an electrogenic membrane transporter, permeable to Na^+, H^+ (OH^-), bicarbonate, borate, and NH_4^+. Recent studies indicate, however, that neither bicarbonate or borate is a substrate. Here, we examined potential NH_4^+, Na^+, and H^+ contributions to electrogenic ion transport through SLC4A11 stably expressed in Na^+/H^+ exchanger-deficient PS120 fibroblasts. Inward currents observed during exposure to NH_4Cl were determined by the $[NH_3]_o$, not $[NH_4^+]_o$, and current amplitudes varied with the $[H^+]$ gradient. These currents were relatively unaffected by removal of Na^+, K^+, or Cl^- from the bath but could be reduced by inclusion of NH_4Cl in the pipette solution. Bath pH changes alone did not generate significant currents through SLC4A11, except immediately following exposure to NH_4Cl. Reversal potential shifts in response to changing $[NH_3]_o$ and pH_o suggested an NH_3/H^+-coupled transport mode for SLC4A11. Proton flux through SLC4A11 in the absence of ammonia was relatively small, suggesting that ammonia transport is of more physiological relevance. Methylammonia produced currents similar to NH_3 but with reduced amplitude. Estimated stoichiometry of SLC4A11 transport was 1:2 (NH_3/H^+). NH_3-dependent currents were insensitive to 10 μM ethyl-isopropyl amiloride or 100 μM 4,4′- diisothiocyanatostilbene-2,2′-disulfonic acid. We propose that SLC4A11 is an $NH_3/2H^+$ co-transporter exhibiting unique characteristics.

SLC4A11 is a recently identified transporter ubiquitously expressed in somatic cells (1, 2), with significant expression in the corneal endothelium, cochlea, and kidney (3). Several SLC4A11 mutations have been implicated in the pathogenesis of Fuchs endothelial corneal dystrophy, congenital hereditary endothelial dystrophy, and Harboyan syndrome (corneal dystrophy with perceptive deafness) (4, 5). Three strains of SLC4A11 knock-out mice exhibited variable phenotypes that included corneal endothelial dysfunction, perceptive deafness, and polyuria or low urine osmolality (6–8). Although SLC4A11 is classified as a member of the SLC4 (solute-linked co-transporter 4) family of bicarbonate transporters, it shares rather low (14–20%) homology with other family members. Phylogenetic analysis of SLC4A11 indicates a separate branch of early evolutionary divergence in the SLC4 family, suggesting a divergent function (9).

Despite high physiological significance of SLC4A11, its transport characteristics remain unclear. Initial studies suggested that SLC4A11 is an electrogenic $2Na^+$-OH^- (or borate) co-transporter (10). However, more recent studies provided evidence that human SLC4A11 transports neither borate nor bicarbonate (9, 11). These studies suggested ethyl-isopropyl-amiloride (EIPA)[3]-sensitive Na^+ and H^+ (or OH^-) permeability through SLC4A11; however, a precise stoichiometry could not be determined. A more recent report has suggested H^+ permeability through SLC4A11 but independent of Na^+ (12).

Interestingly, ammonium permeability (9) and water permeability (13) have also been suggested for SLC4A11, and the across-species highly conserved asparagine-proline-*X* (NP*X*) water channel motif has been identified in a transmembrane domain of SLC4A11 ($N^{639}PS$) (13). Because several water channels, such as AQP3, AQP7, AQP8, AQP9, and AQP10, are ammonia-permeable (14), and a single-point mutation in the aromatic/arginine region (ar/R) can induce ammonia permeability in the ammonia-impermeable water channel AQP1 (15), we hypothesized that SLC4A11 may also exhibit ammonia permeability similar to AQPs. To test this hypothesis, we generated two Na^+/H^+ exchanger (NHE)-deficient Chinese hamster PS120 fibroblast cell lines stably expressing high or low levels of SLC4A11. Employing whole-cell patch clamp electrophysiology, we found that NH_4Cl generated significant EIPA- and 4,4′-diisothiocyanatostilbene-2,2′-disulfonic acid (DIDS)-insensitive currents in SLC4A11-expressing PS120 cells. These currents were sensitive to $[NH_3]$ and $[H^+]$ gradients but were rel-

* This work was supported, in whole or in part, by National Institutes of Health Grants 5R01EY008834 (to J. A. B.), P30EY019008 (Core Grant of Vision Science), and R01HL115140 (to A. G. O). The authors declare that they have no conflicts of interest with the contents of this article.
[1] To whom correspondence may be addressed: 800 Atwater Ave., Bloomington, IN 47405. Tel.: 812-855-4440; E-mail: jbonanno@indiana.edu.
[2] To whom correspondence may be addressed: 635 Barnhill Dr., Rm. 360, Indianapolis, Indiana 46202. Tel: 317-274-8078; E-mail: aobukhov@iu.edu.

[3] The abbreviations used are: EIPA, ethyl-isopropyl-amiloride; AQP, aquaporin; DIDS, 4,4′- diisothiocyanatostilbene-2,2′-disulfonic acid; EV, empty vector; NHE, Na^+/H^+ exchanger; BCECF, 2′7′-bis(carboxyethy)-5(6)-carboxyfluorescein; eNH_4Cl, extracellular NH_4Cl; pF, picofarads; ANOVA, analysis of variance; MA, methylammonia.

atively unaffected by Na^+, K^+, or Cl^- at physiological pH. The displayed current-voltage relations are consistent with an electrogenic NH_3- and H^+-coupled co-transport model.

Experimental Procedures

Transfection and Cell Culture—Human SLC4A11-HA-tagged or empty vector (EV) were stably transfected into NHE-deficient PS120 Chinese hamster CCL39 fibroblast cell line as described previously (9). The SLC4A11 (NP_001167561.1) cDNA was subcloned into a plasmid containing a *neo*^{r} gene for Geneticin G418 selection and a C-terminal HA tag (13). PS120 cells were cultured in DMEM (Gibco®, catalog no. 21063, Life Technologies, Inc.) supplemented with 5% fetal bovine serum (Gibco®, catalog no. 10082, Life Technologies), 1% antibiotic/antimycotic (100 units/ml penicillin and 0.25 μ/ml fungizone), and 1 mg/ml Geneticin® G418 (catalog no. 10131, Life Technologies). The cells were cultured at 37 °C in a 5% CO_2 water-jacketed incubator. Culture medium was changed every other day.

Western Blot—SLC4A11- or EV- PS120 cells were grown on 6-well plates for 3 days before protein extraction. Cells were rinsed with ice-cold PBS, scrapped off from the wells, and sonicated in ice-cold radioimmune precipitation assay buffer (50 mM Tris base, 150 mM NaCl, 0.5% deoxycholic acid-sodium salt, 2% SDS, and 1% Nonidet P-40, pH 7.5) supplemented with complete protease inhibitor mixture (Roche Diagnostics, Mannheim, Germany). The extract was centrifuged for 20 min at 12,000 rpm at 4 °C, and the supernatant was collected. Protein concentration was determined using the 280-nm absorbance assay with a NanoDrop spectrophotometer (Thermo Scientific, Rockford, IL). Protein (15 μg/well) in Protein Loading Buffer Blue (2×) (National Diagnostics, catalog no. EC-886, Atlanta, GA) was resolved on 9% SDS-polyacrylamide gels and wet-transferred to PVDF membranes (Bio-Rad). Membranes were blocked with 5% nonfat milk in TBST (25 mM Tris base, 137 mM NaCl, 0.1% Tween 20) and probed with primary antibodies in the same buffer overnight at 4 °C. The following primary antibodies were used: 1) rabbit polyclonal anti-SLC4A11 (1:1000; 16B12, Covance); 2) mouse monoclonal anti-HA (1:2000; Santa Cruz Biotechnology); or 3) mouse monoclonal α-tubulin antibody (1:5000; DM1A, Novus Biologicals). Next, membranes were probed with secondary antibody (goat anti-mouse IgG peroxidase-conjugated antibody, 1:5000, catalog no. A8924 (Sigma) or goat anti-rabbit IgG peroxidase-conjugated antibody, 1:5000, catalogue no. A0545 (Sigma)) for 1 h at room temperature. Bound secondary antibodies were detected using an enhanced chemiluminescence assay (Supersignal West Pico, Pierce). Band densities and background were quantified using UN-SCAN-IT gel 6.1 (Silk Scientific).

Intracellular pH Measurements—Intracellular pH measurements were performed as described previously (9). Briefly, PS120 cells were cultured on poly-L-lysine-coated 25-mm diameter glass coverslips (Neuvitro Corp., El Monte, CA) for 2–3 days. Before each experiment, cells were incubated with 10 μM pH-sensitive fluorescent dye 2′7′-bis(carboxyethy)-5(6)-carboxyfluorescein (BCECF)-acetoxymethyl ester (Molecular Probes, Inc., Eugene, OR) in Ringer's solution for 30 min at room temperature and washed in dye-free Ringer's solution for another 30 min. The Ringer's solution contained 143.5 mM Na^+, 4 mM K^+, 0.6 mM Mg^{2+}, 1.4 mM Ca^{2+}, 118 mM Cl^-, 1 mM HPO_4^{2-}, 10 mM HEPES, 30 mM gluconate$^-$, and 5 mM glucose, pH 7.5. Na^+-free Ringer's solution contains 143.5 mM $NMDG^+$ instead of Na^+. All of the experimental solutions were equilibrated with air and adjusted to pH 7.5 with 1 N NaOH at 37 °C. Osmolarity of all solutions was adjusted to 295–300 mosM with sucrose. Coverslips with subconfluent cells were mounted into a perfusion chamber. The chamber was then placed on a stage warmer (37 °C) of an inverted microscope (Eclipse TE200, Nikon, Japan). Solutions were kept at 37 °C in a warming box, and the flow of the perfusate (~0.5 ml/min) was achieved by gravity. Cells were imaged with an oil immersion objective (×40; Nikon). BCECF fluorescence was excited alternately at 495 ± 10 and 440 ± 10 nm, and the emitted light was collected through a bandpass filter (520–550 nm). Fluorescence ratios (495 nm/440 nm) were obtained at 1 Hz and converted into pH_i using the high K^+/nigericin calibration approach (16).

TABLE 1
Composition of extracellular solutions

	E1	E2	E4 (0 K^+)	E5 (0 Na^+, 0 K^+)	E6 (0 Cl^-, 0 K^+)	E8
	M	*M*	*M*	*M*	*M*	*M*
NaCl	143.5	45	143.5			80
NMDG-Cl		98.5		143.5		100
K_2HPO_4	1					
KCl	3					
Calcium gluconate	1.4	1.4	1.4	1.4	1.4	1.4
$MgCl_2$	1.22	1.22	1.22	1.22	1.22	1.22
HEPES	10	10	10	10	10	10
Glucose	5.1	5.1	5.1	5.1	5.1	5.1
$NaMeSO_3$					143.5	

Electrophysiological Recordings of PS120 Cells—SLC4A11- and EV-PS120 cells were cultured on 25-mm glass coverslips as described above to ~10–20% confluence. High expression Col4 SlC4A11-PS120 cells were used in all electrophysiology experiments. Whole-cell currents were amplified using an EPC7 amplifier controlled by pCLAMP 10 software (Molecular Devices, Sunnyvale, CA) in the episodic mode. The holding potential was set to −60 mV unless otherwise indicated. The currents were filtered at 3 kHz and sampled at 1 kHz. Each episode lasted 2 s and included a 100-ms voltage ramp from −100 to +100 mV. Series resistance compensation was set at 50%. CLAMPFIT 10 software (Molecular Devices, Sunnyvale, CA) was used for data analysis. Only recordings obtained with a series resistance of less than 10 megaohms were analyzed. Background currents were subtracted when analyzing current amplitude and consequent current density data. No background current subtraction was done when the reversal potential values were determined. The liquid junction potential was subtracted before reporting reversal potential values. An agar salt bridge was used to connect reference electrode and the bath to minimize possible Ag/AgCl reference electrode potential changes during solution exchanges. Complete solution exchange required about 10–15 s in the recording chamber used for electrophysiological experiments (22–23 °C).

Solutions for Electrophysiology—The compositions of extracellular (E) and pipette (intracellular; I) solutions are listed in Tables 1 and 2, respectively. Extracellular solutions were adjusted to desired pH (pH 6.5, 7.5, and 8.5) with 1 N HCl, 1 N

TABLE 2
Composition of intracellular solutions

	I1	I1-NH_4	I2
	mM	*mM*	*mM*
$CsMeSO_3$	125	125	145
$CaCl_2$	5	5	
CsCl			10
$MgCl_2$	2	2	2.2
HEPES	10	30	10
EGTA	10	10	0.5
NH_4Cl		10	
pH	7.2	7.2	7.2

NaOH, or 1 M NMDG base solution (for Na^+-free E5). Intracellular solution pH was adjusted with tris(hydroxymethyl)-aminomethane base to pH 7.2. Osmolality of all solutions was adjusted to 300–310 mosM with mannitol. 10 mM NH_4Cl, methylammonium, tetraethylammonium, or 5 mM $(NH_4)_2SO_4$ salt was added fresh at the day of the experiment. The $(NH_4)_2SO_4$ salt was used instead of NH_4Cl for Cl^--free E6 solution. Equal 0.17 mM NH_3, pH 6.5, pH 7.5, and pH 8.5 E2 solutions were made by equal molar substitution of NMDG-Cl in base E2 solution by 98.5 mM, 10 mM, and 1.16 mM NH_4Cl, respectively. Solution E8 was used to make 1, 3, 10, 30, and 100 mM NH_4Cl extracellular solutions by equal molar substitution of NMDG-Cl with NH_4Cl.

Statistical Analysis—Statistical analysis was performed using SPSS Statistics version 21 (IBM Corp., Armonk, NY). Stoichiometry data were fitted to linear regression in SigmaPlot version 12 (Systat Software Inc., San Jose, CA). Throughout, data are presented as mean ± S.E., in which significance level is indicated as follows: $p < 0.05$ (*), $p < 0.01$ (**), and $p < 0.001$ (***).

Results

Ammonium Permeability through SLC4A11 Is Expression-dependent—Previously, using BCECF pH_i measurements, we observed increased Na^+ and NH_4^+ permeability and higher capacity to recover from acid loads in SLC4A11-expressing HEK293 or PS120 cells (9). To further clarify the underlying mechanisms, we generated two stably transfected PS120 cell lines (Na^+/H^+ exchanger-deficient), high expression colony 4 (Col4) and low expression colony 12 (Col12). We determined, by Western blot, that Col4 expressed 1.34 times more SLC4A11 than Col12 (anti-HA; Fig. 1*A*), whereas no endogenous SLC4A11 can be detected in EV-PS120 cells (anti-SLC4A11; Fig. 1*A*). Employing these two colonies of SLC4A11-PS120 cells, we examined the pH_i response to extracellular 10 mM NH_4Cl, relative to EV. Fig. 1*B* shows that NH_4Cl application caused a rapid pH_i rise in both SLC4A11-PS120 and EV-PS120 (labeled *a*) due to NH_3 gas diffusion and intracellular production of NH_4^+ and OH^- (17). In phase *b*, pH_i plateaued in EV-PS120 cells (−0.01 ± 0.02 ΔpH/Δmin), whereas a significant acidification occurred in SLC4A11-PS120 cells. The acidification rate (ΔpH/Δmin) was 1.57 times higher in Col4 (−0.11 ± 0.02, $n = 3$) than in Col12 cells (−0.07 ± 0.01, $n = 3$) (Fig. 1*C*). Removing NH_4Cl (phase *c*) caused a prominent acidification: ΔpH_i −0.68 ± 0.10 in Col4 ($n = 3$) and 1.55 times less ΔpH_i −0.44 ± 0.03 in Col12 ($n = 3$), whereas essentially no acidification occurred (−0.08 ± 0.04, $n = 5$) in EV-PS120 cells

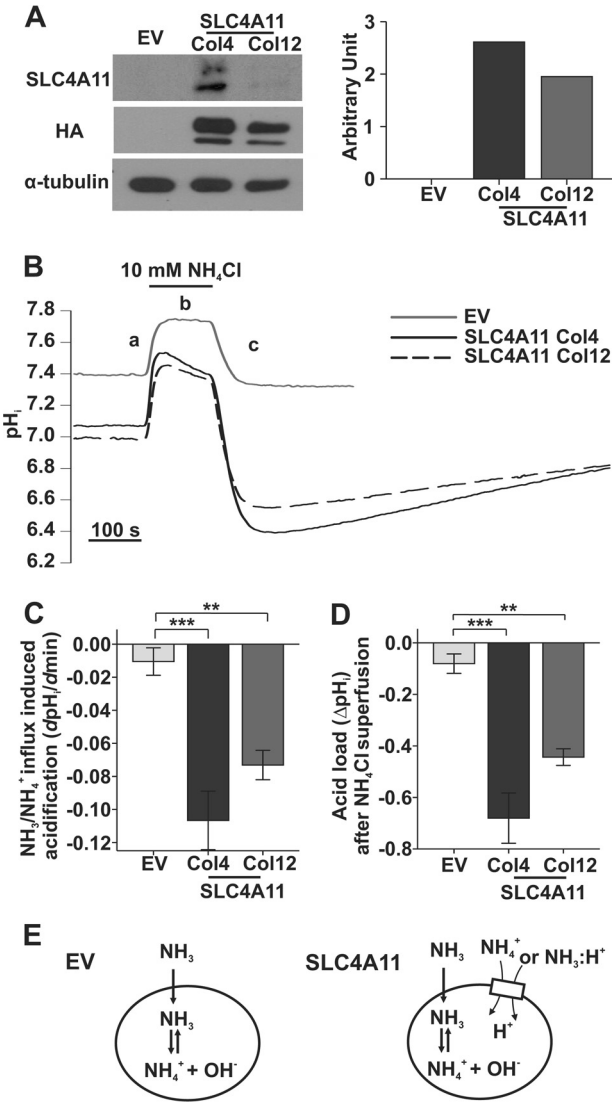

FIGURE 1. **NH_4Cl superfusion induced differential intracellular acidification in SLC4A11-PS120 relative to EV-PS120 cells.** *A*, Western blot verification of SLC4A11 expression in EV (empty vector), Col4, and Col12 using anti-SLC4A11 and anti-HA antibodies. A doublet shows glycosylated and non-glycosylated forms of SLC4A11 protein (40). The bar graph on the *right* shows the density quantification of HA-SLC4A11 normalized to α-tubulin. *B*, pH_i response to 10 mM NH_4Cl pulse in EV and SLC4A11 PS120 cells. Each trace is the average of $n = 5$ EV, $n = 3$ SLC4A11 Col4, and $n = 3$ SLC4A11 Col12, respectively. The *traces* show the rapid alkalinization phase (*a*), slow acidification phase (*b*), and rapid acid loading phase (*c*). *C*, phase *b* apparent ammonium influx ($\Delta pH_i/\Delta min$) in SLC4A11 Col4 ($n = 3$, $p = 0.001$) and Col12 ($n = 3$, $p = 0.01$) is higher than in the EV control ($n = 5$) (one-way ANOVA with Tukey honest significant difference post hoc test, $p = 0.001$). *D*, phase *c* ammonium-induced peak acidification (ΔpH_i) during wash is higher in SLC4A11 Col4 ($n = 3$, $p < 0.001$) and Col12 ($n = 3$, $p = 0.004$) than in the EV control ($n = 5$) (one-way ANOVA with Tukey honest significant difference post hoc test, $p < 0.001$). *E*, *left*, *EV*, simple NH_3 diffusion equilibrates and raises pH_i (phase *a* in Fig. 1*B*), but no secondary acidification occurs due to lack of NH_4^+ permeability (phase *b*). *Right*, *SLC4A11*, NH_3 diffusion caused similar pH_i rise as in EV (phase a); additional NH_4^+ (or NH_3-H^+) permeability from SLC4A11 adds net H^+ influx and causes gradual acidification (phase *b*). *Error bars*, S.E. **, $p < 0.01$; ***, $p < 0.001$.

(Fig. 1*D*). Phase *b* acidification is generally attributed to a finite permeability to NH_4^+, and consequent phase *c* acidification is a H^+ loading effect from the finite NH_4^+ permeability in phase *b* (17). The extents of acidification during phases *b* and *c* were both positively associated with the SLC4A11 expression level

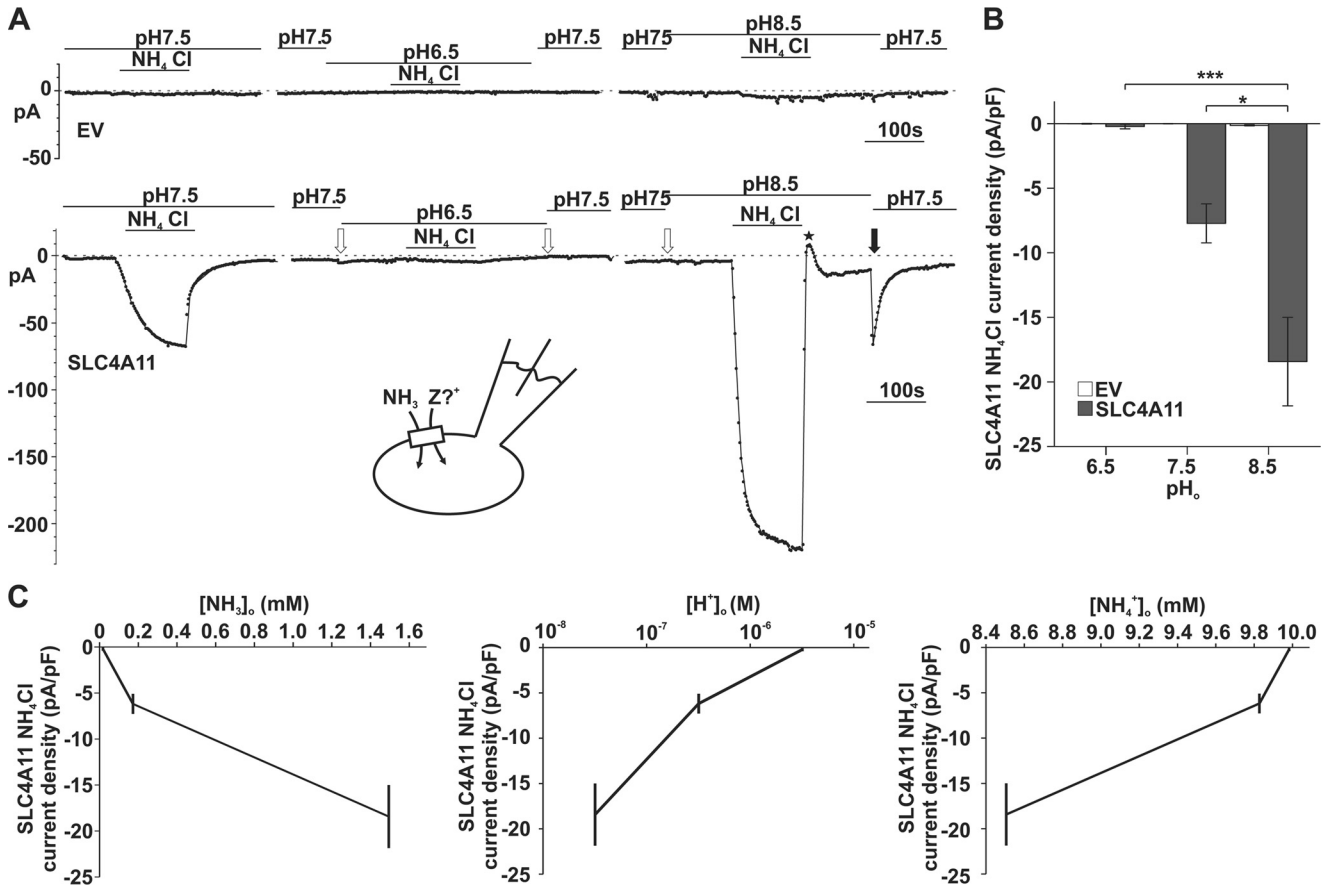

FIGURE 2. **eNH$_4$Cl-dependent inward currents through SLC4A11.** *A*, sample trace of whole-cell current recording (−60 mV holding potential) in response to 10 mM eNH$_4$Cl at pH$_o$ 6.5, 7.5, and 8.5 in EV- (*top trace*) and SLC4A11-PS120 cells (*bottom trace*). Bath pH changes themselves did not elicit significant currents (*open arrows*). A pH 8.5 wash after pH 8.5 NH$_4$Cl elicited outward current (*star*), and the pH 8.5 to 7.5 transition after NH$_4$Cl pulse elicited inward currents (*filled arrow*). *Inset*, schematic diagram showing currents carried by NH$_3$ and an unknown charge carrier by SLC4A11. *B*, bar graph summary of NH$_4$Cl-dependent current density in EV ($n = 3$) and SLC4A11 cells ($n = 4$) (repeated measure ANOVA, cell type, $p = 0.005$; pH, $p = 0.009$; Tukey honest significant difference post hoc test comparing currents at pH 6.5 *versus* pH 7.5, pH 7.5 *versus* pH 8.5, and pH 6.5 *versus* pH 8.5, $p = 0.085$, 0.001, and 0.017, respectively). *C*, SLC4A11 inward current density *versus* extracellular [NH$_3$], [H$^+$], or [NH$_4^+$] in 10 mM NH$_4$Cl at pH 6.5, 7.5, and 8.5. NH$_4^+$ pK_a 9.25 was used for concentration calculation. *Error bars*, S.E. *, $p < 0.05$; ***, $p < 0.001$.

(Fig. 1, *C* and *D*). Thus, we reasoned that SLC4A11 expression increased the apparent NH_4^+ permeability in PS120 cells. This permeability could be solo NH_4^+ transport or co-transport of NH_3-H^+ (14), but it cannot be differentiated by BCECF pH$_i$ measurements.

[NH$_3$]$_o$ Not [NH$_4^+$]$_o$ Drives Extracellular NH$_4$Cl (eNH$_4$Cl)-dependent Inward Currents through SLC4A11—A previous study provided evidence that SLC4A11 may function as an electrogenic transporter in SLC4A11-HEK293 cells (10). Therefore, we next used the whole-cell patch clamp approach to determine whether the apparent NH_4^+ (or NH_3-H^+) permeability creates charge movements by applying 10 mM eNH$_4$Cl to SLC4A11-PS120 Col4 cells. NH$_4$Cl solutions were adjusted to three different extracellular pH levels (7.5, 6.5, and 8.5) to vary the proportion of NH_3 to NH_4^+. No currents were observed in EV-PS120 during any of these NH$_4$Cl exposures (Fig. 2*A*, *top*). In contrast, in SLC4A11-PS120 shown in Fig. 2*A* (*bottom*), pH 7.5 eNH$_4$Cl application caused inward currents of −6.18 ± 1.09 pA/pF, ($n = 7$), whereas pH 6.5 eNH$_4$Cl induced significantly smaller inward currents (−0.22 ± 0.19 pA/pF, $n = 4$), and pH 8.5 eNH$_4$Cl elicited markedly larger inward currents (−18.43 ± 3.43 pA/pF, $n = 4$. Fig. 2*B* shows a summary bar graph of current density for EV- and SLC4A11-PS120 cells. In Fig. 2*C*, we plotted the current density against [NH$_3$]$_o$ (*left*), [H$^+$]$_o$ (*middle*), and [NH$_4^+$]$_o$ (*right*), respectively. The eNH$_4$Cl-dependent current density varied directly with [NH$_3$]$_o$ but inversely with [H$^+$]$_o$ or [NH$_4^+$]$_o$. From pH 6.5 to 8.5, the 84-fold increase in current density was concomitant with a 75-fold increase in [NH$_3$]$_o$; conversely, there was essentially no change (17% decrease) in [NH$_4^+$]$_o$ and a 100-fold decrease in [H$^+$]$_o$.

These results suggest that NH$_3$ is the actual transported species and that the [NH$_3$] gradient contributes to the driving force in SLC4A11 transport. To further test this hypothesis, we adjusted the NH$_4$Cl concentration to achieve equal [NH$_3$]$_o$ = 0.17 mM in the three different pH solutions. This required 98.5 mM NH$_4$Cl in the pH 6.5 E2 solution, 10 mM NH$_4$Cl in pH 7.5 E2, and 1.16 mM NH$_4$Cl in pH8.5 E2, calculated from NH_4^+ pK_a = 9.25 (equal molar substitution with NMDG-Cl). Fig. 3*A* shows a sample trace of current recording, and Fig. 3*B* shows the summary bar graph of current density. In this series, with [NH$_3$] being equal (0.17 mM), we observed similar amplitude in current density under pH 6.5 and 8.5 compared with pH 7.5. This result strongly supports the notion that [NH$_3$]$_o$ rather than [NH$_4^+$]$_o$ drives the inward currents through SLC4A11. Interest-

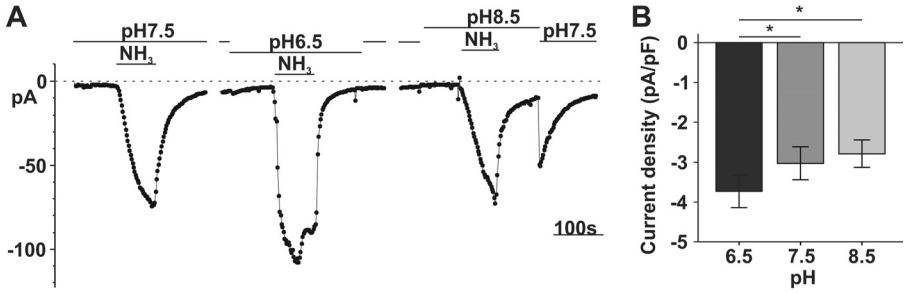

FIGURE 3. **eNH$_4$Cl-dependent inward currents when holding [NH$_3$]$_o$ constant in SLC4A11-PS120.** *A*, sample current trace in response to 0.17 mM NH$_3$ at pH$_o$ 6.5, 7.5, and 8.5 in SLC4A11-PS120 cells. Current amplitude is similar across three pH solutions, with slightly larger current in pH 6.5 and slightly smaller current at pH 8.5. *B*, bar graph summary of NH$_3$/H$^+$ maximum current density at pH 6.5, 7.5, and 8.5 after a 40-s exposure to NH$_4$Cl. Current density shows small differences under the three pH conditions, largest in pH 6.5 NH$_3$ and smallest in pH 8.5 ($n = 3$, repeated measure ANOVA, $p = 0.001$; pairwise comparison pH 6.5 *versus* pH 7.5, $p = 0.022$; pH 7.5 *versus* pH 8.5, $p = 0.051$; pH 6.5 *versus* pH 8.5, $p = 0.012$). *Error bars*, S.E. *, $p < 0.05$.

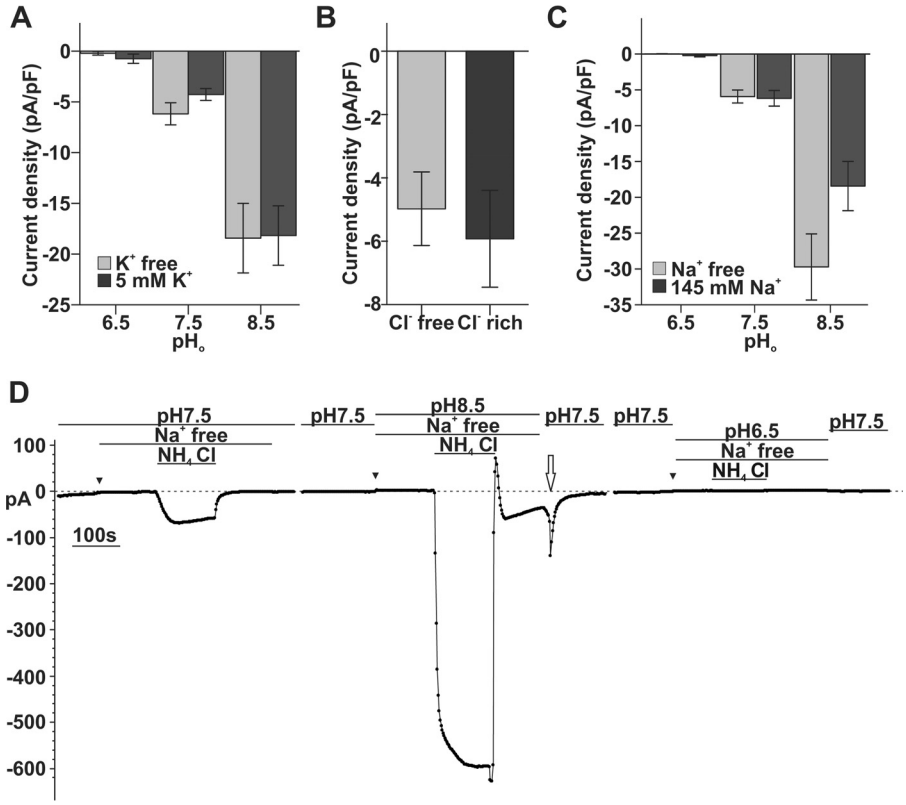

FIGURE 4. **K$^+$, Cl$^-$, and Na$^+$ are not substrates for SLC4A11 under physiological pH.** *A*, the eNH$_4$Cl-dependent current is not affected by removal of extracellular K$^+$ at pH 6.5, 7.5, and 8.5. Sample size (*n*) under each condition is as follows: K$^+$-free, pH 6.5, $n = 4$; pH 7.5, $n = 7$; pH 8.5, $n = 4$; 5 mM K$^+$, pH 6.5, $n = 3$; pH 7.5, $n = 6$; pH 8.5, $n = 4$ (factorial ANOVA, 5 mM K$^+$ *versus* K$^+$-free, $p = 0.716$; K$^+$/pH interaction, $p = 0.763$). *B*, the eNH$_4$Cl-dependent current is not affected by removal of extracellular Cl$^-$ at pH 7.5. (Cl$^-$-free $n = 5$ *versus* Cl$^-$-rich $n = 6$; independent *t* test, $p = 0.645$). *C*, bar graph shows that eNH$_4$Cl-dependent current is not affected by removal of extracellular Na$^+$ at pH 6.5 and 7.5 but is enhanced at pH 8.5. Sample size (*n*) under each condition is as follows: Na$^+$-free, pH 6.5 $n = 4$, pH 7.5 $n = 6$, and pH 8.5 $n = 6$; 145 mM Na$^+$, pH 6.5 $n = 4$, pH 7.5 $n = 7$, and pH 8.5 $n = 4$ (factorial ANOVA, Na$^+$ *versus* Na$^+$-free, $p = 0.108$; Na$^+$/pH interaction, $p = 0.058$). *D*, sample trace of whole-cell recording to test Na$^+$ sensitivity. Removal of Na$^+$ does not significantly change eNH$_4$Cl-dependent current and slightly reduces baseline current (*triangles*). Bath pH transition after pH 8.5 NH$_4$Cl elicited inward current (*open arrow*). *Error bars*, S.E.

ingly, further analysis of current density revealed small differences between each pH condition ($n = 3$; repeated ANOVA, $p = 0.001$). It appears that [H$^+$] gradients or extracellular pH affects SLC4A11 activity, whereas the inward current density is primarily determined by [NH$_3$]$_o$.

SLC4A11 eNH4Cl-dependent Current Is Independent of K$^+$, Cl$^-$, and Na$^+$—Given that NH$_3$ is an uncharged molecule, we next tested whether K$^+$, Cl$^-$, or Na$^+$ is the charge carrier of the eNH$_4$Cl-dependent currents. Refer to Table 2 for solution composition. Removal of K$^+$ (E1 K$^+$ *versus* E4 K$^+$-free) had no effect on eNH$_4$Cl-dependent currents at pH 6.5, 7.5, and 8.5 (Fig. 4*A*; factorial ANOVA, $p = 0.716$). Similarly, removal of extracellular Cl$^-$ (5 mM $(NH_4)_2SO_4$ was added in both Cl$^-$-free E6 and Cl$^-$-rich E4 solutions for comparison) did not affect the eNH$_4$Cl-dependent current at pH 7.5 (independent *t* test, $p = 0.65$; Fig. 4*B*). Removal of Na$^+$ (E4 Na$^+$-rich *versus* E5 Na$^+$-free) did not significantly affect eNH$_4$Cl-dependent currents at pH 6.5 or 7.5 (Fig. 4*C*; factorial ANOVA Na$^+$, $p = 0.108$; Na$^+$/pH interaction, $p = 0.058$), but interestingly, the absence of Na$^+$ enhanced eNH$_4$Cl-dependent inward currents by 38% at pH 8.5 (Fig. 4, *C* and *D*). At pH 8.5, eNH$_4$Cl-dependent current density in 143.5 mM Na$^+$ E4 was -18.43 ± 3.43 pA/pF ($n =$

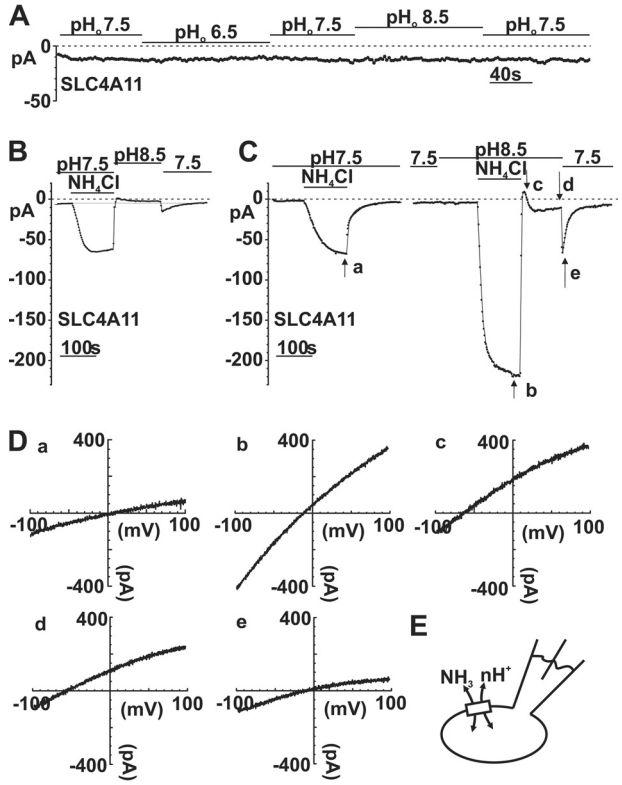

FIGURE 5. **Current-voltage relations of eNH$_4$Cl-dependent SLC4A11 currents.** *A*, sample trace showing that bath pH transitions do not generate significant currents in the absence of NH_4Cl. *B*, sample trace showing that transient outward current was induced after pH 7.5 eNH_4Cl by a pH 8.5 wash, and transient inward currents were elicited during pH 8.5 → 7.5 bath transition. *Light gray line*, baseline current. *C*, same trace as in Fig. 2*A*, highlighting points for E_{rev} comparisons. *D*, corresponding *I*-*V* plot at the time points *a*, *b*, *c*, *d*, and *e*. *E*, schematic diagram showing current in SLC4A11 cells is carried by NH_3 and an unknown charge ion.

4), whereas it was −29.71 ± 4.62 pA/pF ($n = 6$) in Na^+-free E5 (independent *t* test, $p = 0.115$; Fig. 4*C*). In summary, it is unlikely that K^+, Cl^-, or Na^+ carries the eNH_4Cl-dependent currents. However, there is some interaction with Na^+ at high pH_o.

SLC4A11 Co-transports NH_3 and H^+—In Fig. 2*A* (*bottom trace*, *solid arrow*) and Fig. 4*D* (*open arrow*), we observed inward current induced by a bath pH decrease (8.5 → 7.5) after a pH 8.5 NH_4Cl pulse, suggesting that SLC4A11 can provide H^+ conductance. Fig. 3 shows that $[H^+]_o$ affects SLC4A11 inward current density and kinetics in the presence of NH_3. Fig. 5*A* (and Figs. 2*A* and 4*D*), however, shows that simple bath pH changes do not induce noticeable current. These data suggest that H^+ current is only measurable when there is NH_3 present. In Fig. 2*A*, a pH 8.5 wash after pH 8.5 NH_4Cl pulse induced an outward current (labeled with a *star*). We reasoned that this outward current is the efflux of NH_3 coupled to H^+ resulting from outward NH_3 and H^+ gradient during wash. To validate, we applied a pH 8.5 wash following a pH 7.5 NH_4Cl pulse, creating a greater outward $[H^+]$ gradient than a pH 7.5 wash. Fig. 5*B* shows smaller but measureable outward current (relative to the initial baseline) during this pH 8.5 wash, supporting the notion of NH_3-coupled H^+ efflux. In contrast, no outward current is observed during a pH 7.5 wash after pH 7.5 eNH_4Cl pulse, indicating that an outward H^+ gradient is needed. Fig. 5*C* (*right trace*) shows that later in the same cell, a pH 8.5 eNH_4Cl pulse was followed by a pH 8.5 wash. The outward current (point *c*) during the wash is consistent with outward gradients of both $[NH_3]$ and $[H^+]$. Interestingly, a return to pH 7.5 bath produced a significant inward current (point *e*), consistent with an increased $[H^+]$ inward gradient. These data show that significant H^+ current through SLC4A11 can occur after an NH_4Cl pulse.

To provide further insight into this potential NH_3-H^+ co-transport model, we examined the reversal potentials at key points in Fig. 5*C*. The liquid junction potential was estimated to be 8.9 mV in this E4-I1 solution pairing and was subtracted from raw E_{rev} values before analysis. Fig. 5*D* (*a*) shows the *I*-V relation at point *a* in Fig. 5*C*. The E_{rev} was −4.16 ± 1.47 mV ($n = 10$), inconsistent with solo NH_4^+ conductance, which will otherwise result in large positive E_{rev} (14). Furthermore, we analyzed E_{rev} at time points *b*, *c*, *d*, and *e* (during and after pH 8.5 NH_4Cl pulse). Fig. 5*D* (*b*), during pH 8.5 NH_4Cl, E_{rev} was −21.56 ± 1.98 mV ($n = 4$) at the inward current peak. Ten seconds into the pH 8.5 wash (point *c*), E_{rev} shifted to −66.24 ± 2.03 mV ($n = 4$). Assuming that $[H^+]_o$, $[H^+]_i$, and $[NH_3]_i$ changed very little from *b* to *c* in this short time frame, the decreasing $[NH_3]_o$ should result in a left shift of E_{rev} to a more negative value and result in outward current. Indeed, we observed a negative shift in E_{rev} and NH_3-H^+ outward currents, representing efflux of NH_3-H^+ following NH_3 and H^+ outward gradient. Returning to pH 7.5 bath, E_{rev} shifted from −66.37 ± 2.23 mV ($n = 4$, point *d*) to −37.60 ± 5.30 mV ($n = 4$, point *e*). This E_{rev} rightward shift was induced by increased $[H^+]$inward gradient and resulted in inward currents. In summary, these data suggest that $[NH_3]$ and $[H^+]$ changes synergistically affect current direction and apparent E_{rev} in SLC4A11-PS120 cells, supporting the hypothesis that NH_3 and H^+ are transported in a coupled manner.

SLC4A11 H^+ Permeability in the Absence of Ammonia Is Very Small—Fig. 1*B* suggests that the resting pH_i in SLC4A11-transfected cells is lower than EV. Analysis of data from more cells (Fig. 6*A*) shows that the resting pH_i was significantly lower in SLC4A11-PS120 Col4 (pH_i 6.98 ± 0.08, $n = 20$) relative to EV-PS120 (pH_i 7.32 ± 0.08, $n = 23$), suggesting that SLC4A11 provides some H^+ permeability in the absence of NH_3, where a negative membrane potential could drive H^+ influx, as proposed in a recent report (12). Figs. 2*A* and 5*A*, however, do not reveal any measureable H^+ currents in the absence of NH_3. Nevertheless, increased H^+ permeability is evident in SLC4A11-transfected cells during the acid recovery following NH_4Cl pulses in previous reports (9, 12). Fig. 6*B* shows that acid recovery rates after NH_4Cl pulse were significantly greater in Col4 and Col12 cells relative to EV. Next, to avoid cell exposure to NH_3, we used sodium acetate to acidify these cells and monitored acid recovery. Fig. 6, *C* and *D*, show a similarly enhanced acid recovery in SLC4A11 transfected cells during acidification with sodium acetate, indicating that this apparent H^+ permeability is independent of NH_3. The H^+ efflux during sodium acetate experiments was 4.7 μM/s ($\Delta pH/\Delta s \times 14$ mM/pH buffering capacity), similar to that reported recently for SLC4A11 H^+ permeability (12). However, this efflux rate is quite small, only about 2.4% of Na^+/H^+ exchanger 1 (NHE1)-facilitated H^+

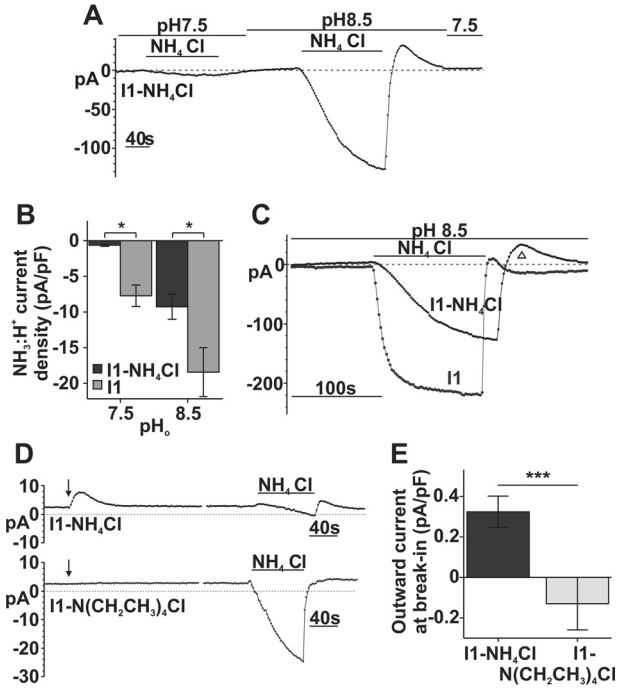

FIGURE 6. **H^+ permeability through SLC4A11 in the absence of NH_3 is small.** *A*, baseline pH_i in SLC4A11-PS120 cells (6.98 ± 0.37, $n = 20$) is significantly lower than in EV-PS120 cells (7.32 ± 0.41, $n = 23$) (independent *t* test, $p = 0.008$). *B*, acid recovery rates following NH_4Cl pulses (see Fig. 1) in Col4 ($n = 3$) and Col12 ($n = 3$) SLC4A11-expressing cells relative to EV ($n = 5$). (one-way ANOVA, $p = 0.001$; post hoc Bonferroni EV *versus* Col4, $p = 0.001$; EV *versus* Col12, $p = 0.012$). *C*, pH_i response to sodium acetate in EV and SLC4A11 cells. *D*, bar graph summary of acid load recovery rate in SLC4A11- ($n = 4$) or EV-PS120 ($n = 4$) cells during 40 mM sodium acetate pulse (independent *t* test, $p = 0.011$). *Error bars*, S.E. *, $p < 0.05$; **, $p < 0.01$; ***, $p < 0.001$.

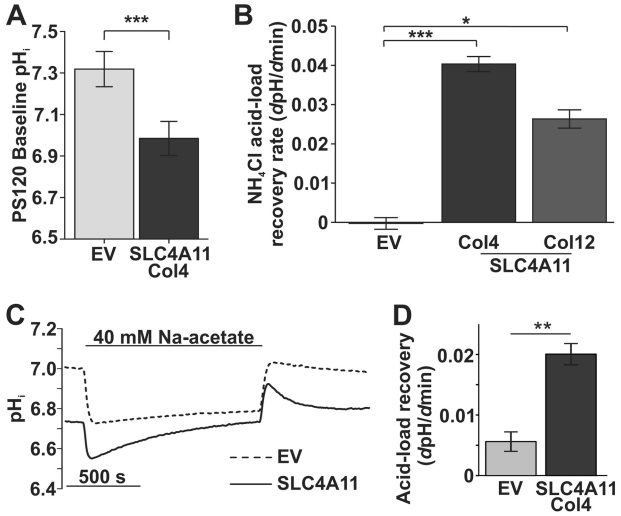

FIGURE 7. **eNH$_4$Cl-dependent currents through SLC4A11 are sensitive to transmembrane [NH_3] gradient.** *A*, sample trace of a whole-cell current recording in SLC4A11 cells with intracellular 10 mM NH_4Cl and 10 mM eNH_4Cl superfusion at −60 mV holding potential. *B*, bar graph summary of responses to eNH_4Cl in I1-NH_4Cl- ($n = 3$) *versus* I1-dialyzed cells ($n = 4$) (repeated measure ANOVA; intracellular NH_4Cl, $p = 0.03$; in NH_4Cl/pH interaction, $p = 0.610$). *C*, overlay of NH_3/H^+ current development in I1-NH_4Cl and I1 pipette solution. Data were fitted to a standard exponential equation, $\tau = 58.44 \pm 17.58$ s for I1-NH_4Cl ($n = 3$) *versus* $\tau = 9.00 \pm 0.88$ s for I1 ($n = 4$) (independent *t* test, $p = 0.02$, equal variance not assumed). *D*, representative trace of whole-cell current recording in SLC4A11-PS120 cells with intracellular 10 mM NH_4Cl or $N(CH_2CH_3)_4Cl$ at break-in (*arrows*) and during 10 mM eNH_4Cl superfusion at −10 mV holding potential. *E*, bar graph summary of break-in outward current density in cells with I1-NH_4Cl ($n = 7$), or I1-$N(C_2H_5)_4Cl$ ($n = 4$) (independent *t* test, $p = 0.009$). *Error bars*, S.E. *, $p < 0.05$; ***, $p < 0.001$.

flux (0.2 mM/s) (19), and ~7.3 times smaller than H^+ flux in NH_4Cl (see Fig. 1*C*). Moreover, the effects of this added H^+ permeability on resting pH_i are not evident in bicarbonate-rich conditions (*i.e.* high buffering capacity) (9, 12) or NHE-expressing cells (9).

Intracellular NH_3 Decreases SLC4A11 NH_3/H^+ Inward Currents—Fig. 5*C* (*d*) demonstrates that an outward $[NH_3]$ gradient can produce an outward current in SLC4A11-PS120 cells. Therefore, we next tested whether reversing or dissipating the transmembrane $[NH_3]$ gradient by increasing intracellular $[NH_3]$ would reverse any SLC4A11 electrogenic activity. Previously, we used a standard pipette solution containing 0 mM NH_4Cl (I1), whereas here we used 10 mM NH_4Cl pipette solution (I1-NH_4Cl). Liquid junction potential was estimated to be 8.5 mV in this E4-I1-NH_4Cl solution pairing and was subtracted from raw E_{rev} values before analysis.

We dialyzed I1-NH_4Cl into SLC4A11-PS120 cells reversing the transmembrane $[NH_3]$ gradient, hoping this would be sufficient to stimulate outward current. However, when the cell was held at −60 mV, we observed no significant current at pH 7.5 or 8.5 (E4 bath solution) (Fig. 7*A*). During NH_4Cl application, inward current (Fig. 7*A*) was smaller than that with standard 0 mM $[NH_3]$ intracellular solution. Fig. 7*B* shows current densities amounting to −0.63 ± 0.16 pA/pF ($n = 3$) at pH 7.5 NH_4Cl and −9.26 ± 1.73 pA/pF at pH 8.5 NH_4Cl ($n = 3$); both were significantly smaller than that in I1 dialysis ($p = 0.03$), consistent with a reduced driving force for NH_3-H^+ inward currents because of reduced $[NH_3]_o/[NH_3]_i$ gradient. Interestingly, the presence of intracellular NH_3 and/or the reduced NH_3 gradient also slows current development. Fig. 7*C* shows a significant difference in the time constants between I1-NH_4Cl, $\tau = 58.44 \pm 17.58$ s ($n = 3$), and I1, $\tau = 9.00 \pm 0.88$ s ($n = 4$). In addition, the outward current at the pH 8.5 wash was prolonged and more prominent with I1-NH_4Cl dialysis than I1 (Fig. 7*C*, △), indicating that increased $[NH_3]_i$ can produce larger outward current.

Whereas we could not see outward currents at baseline in I1-NH_4Cl dialysis with −60 mV holding potential, Fig. 7, *D* and *E*, shows that at −10 mV holding potential, outward currents can be seen on break-in (*arrow*). As a control, dialysis of I1-$N(CH_2CH_3)_4Cl$ (tetraethylammonium chloride; Fig. 7*D*, *bottom trace*) did not activate any currents on break-in (*arrow*). (Extracellular $N(CH_2CH_3)_4Cl$ superfusion does not generate currents in SLC4A11-PS120 cells (Fig. 8*D*).) Moreover, Fig. 7*D* shows that inward currents at pH 7.5 NH_4Cl were similarly reduced in an I1-NH_4Cl-dialyzed cell compared with an I1-$N(CH_2CH_3)_4Cl$-dialyzed cell. Also, Fig. 7*D* (*top trace*) shows outward currents at the beginning of the pH 7.5 wash in I1-NH_4Cl-dialyzed cells. This outward current, although small, is consistent with an increased $[NH_3]_i$.

Methylammonia $N(CH_3)H_2$ Can Also Be Transported by SLC4A11—Because ammonia-permeable Rh and AQPs can also transport methylammonia (MA) (20), we next examined whether this ammonia derivative can be transported by SLC4A11. $N(CH_3)H_3Cl$ application produced similar pH-sensitive inward currents, smaller at low pH and larger at high pH

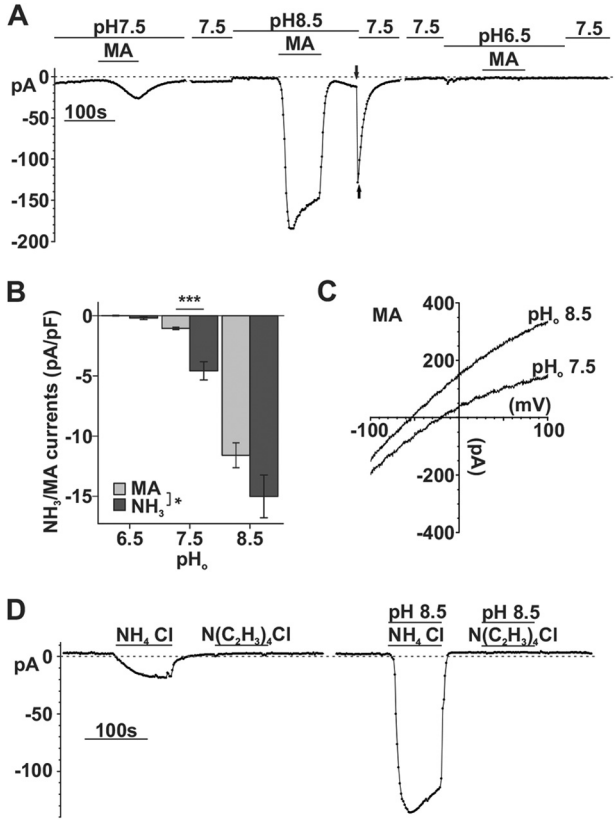

FIGURE 8. **SLC4A11 can also transport methylammonia.** *A*, sample trace of whole-cell current recording in response to extracellular 10 mM MA and change of extracellular pH in SLC4A11-PS120 cells. *B*, bar graph showing a comparison of MA- and NH_3-induced current density in SLC4A11 cells (factorial ANOVA, NH_3 *versus* MA, $p = 0.048$; pH, $p < 0.001$; substrate/pH interaction, $p = 0.498$; independent *t* test comparing NH_3 (*n*) and MA (*n′*) current density at pH 6.5 ($n = 6$ *versus* $n' = 3$), pH 7.5 ($n = 21$ *versus* $n' = 6$), and pH 8.5 ($n = 10$ *versus* $n' = 5$), $p = 0.293$, <0.001, and 0.221, respectively). *C*, representative reversal potential shift after MA perfusion. *D*, sample trace of whole-cell recording showing that tetramethylammoniun $N(C_2H_3)_4Cl$ does not generate currents in SLC4A11-PS120 cells. *Error bars*, S.E. ***, $p < 0.001$.

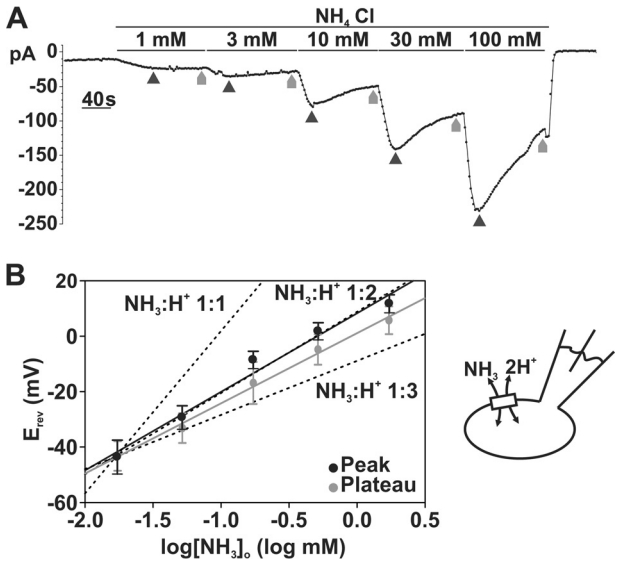

FIGURE 9. **Stoichiometry of SLC4A11 estimated to be 1:2 NH_3/H^+.** *A*, sample trace of whole-cell current recording in response to sequentially increasing extracellular (pH_o 7.5) NH_4Cl concentration in SLC4A11-PS120 cell at −60 mV holding potential. E_{rev} data for maximum "peak" current was obtained at points indicated by *dark black arrows*, whereas E_{rev} for "plateau" currents were obtained at *gray arrows*. *B*, reversal potentials obtained at maximum current ("peak") were plotted against extracellular $log[NH_3]_o$. The plot shows a linear relationship between E_{rev} and $log[NH_3]_o$ with a slope of 28.30 mV/log mM ($r^2 = 0.840$, $p < 0.0001$). *Dashed lines*, predicted NH_3/H^+ 1:1, 1:2, and 1:3 slope. Reversal potentials obtained at "plateau" currents were also plotted against extracellular $log[NH_3]_o$, with a linear slope of 25.24 mV/log mM ($r^2 = 0.699$, $p < 0.0001$). *Error bars*, S.E.

(Fig. 8*A*). Average current densities (pA/pF) at extracellular pH 6.5, 7.5, and 8.5 were -0.01 ± 0.03, -1.05 ± 0.10, and -11.60 ± 1.03, respectively, which were significantly smaller than NH_4Cl-dependent current density ($p = 0.048$). This is consistent with lower free [MA] due to the higher pK_a of MA^+ (pK_a 10.64) than pK_a of NH_4^+ (pK_a 9.25). Fig. 8, *A* and *C*, shows that the transient currents elicited at the pH 8.5 → 7.5 transition after pH 8.5 MA were similar to what was observed with NH_4Cl. The E_{rev} shift from -56.88 ± 3.37 mV ($n = 4$) at pH 8.5 to -24.39 ± 2.93 mV ($n = 4$) at pH 7.5 was also similar to that observed with NH_4Cl. As we indicated above, application of the bulkier tetraethylammonium $N(CH_2CH_3)_4^+$ did not induce any current (Fig. 8*D*), indicating that there is a size limit for substrates of SLC4A11.

SLC4A11 Stoichiometry—We next set out to determine the stoichiometry of NH_3/H^+ transport through SLC4A11 at physiological pH 7.5. According to the equation,

$$E_{rev} = \frac{1}{z_m m + z_n n} \frac{RT}{F} \ln \left(\frac{[NH_3]_o}{[NH_3]_i} \right)^m \left(\frac{[H]_o}{[H]_i} \right)^n \qquad \text{(Eq. 1)}$$

where m is the stoichiometry of NH_3, n is the stoichiometry of H^+, Z_m is the charge of NH_3 ($Z_m = 0$), Z_n is the charge of H^+ ($Z_n = +1$), R is the gas constant 8.314 J/mol*K, F is the Faraday constant 96,485 C/mol, and T is temperature in K (295 K), there is a linear relationship between E_{rev} and $log[NH_3]_o$ with a slope of $\ln(10) \times RT/F \times m/n$ if we assume that $[NH_3]_i$, $[H]_i$, and $[H]_o$ are constant (21). Using this equation, we first predicted the values of linear slopes at each possible m (NH_3)/n (H^+) stoichiometry (at 22 °C): (i) 58.5 mV/log mM if NH_3/H^+ stoichiometry is 1:1; (ii) 29.25 mV/log mM if NH_3/H^+ stoichiometry is 1:2; and (iii) 19.50 mV/log if NH_3/H^+ stoichiometry is 1:3 (*dashed lines* in Fig. 9*B*). We then experimentally determined the E_{rev} of SLC4A11 NH_3/H^+ currents at different $[NH_3]_o$ by sequentially superfusing SLC4A11-PS120 cells with 1, 3, 10, 30, and 100 mM NH_4Cl E8 solutions (I2 pipette solution; Fig. 8*A*). Liquid junction potential was estimated to be 13.8 mV and was subtracted from E_{rev} values before analysis. Using the adjusted E_{rev} at the current peak at each concentration, the plot was linear ($r^2 = 0.840$) with a slope of 28.30 ± 2.78 mV/log mM ($p < 0.0001$), closest to the 1:2 NH_3/H^+ stoichiometry. As shown in Fig. 8*A*, we observed some current decay at higher NH_4Cl concentrations, which could be due to an increased $[NH_3]_i$ leading to decreased $[NH_3]_o/[NH_3]_i$ gradient and in turn diminishing the current and underestimating the actual E_{rev}. To examine this possibility, we also plotted E_{rev} obtained at the eNH_4Cl-current steady-state phase (plateaus). Indeed, we observed decreased E_{rev} values at high NH_4Cl conditions. Fig. 9*B* shows the plot of E_{rev} at plateau *versus* $log[NH_3]_o$. The slope is 25.24 ± 3.46 mV/log mM ($r^2 = 0.699$, $p < 0.0001$) still closest to the 1:2 NH_3/H^+ stoichiometry slope.

NH_3/H^+ current is not sensitive to DIDS or EIPA—Previous reports indicated that EIPA inhibits SLC4A11 Na^+-H^+ perme-

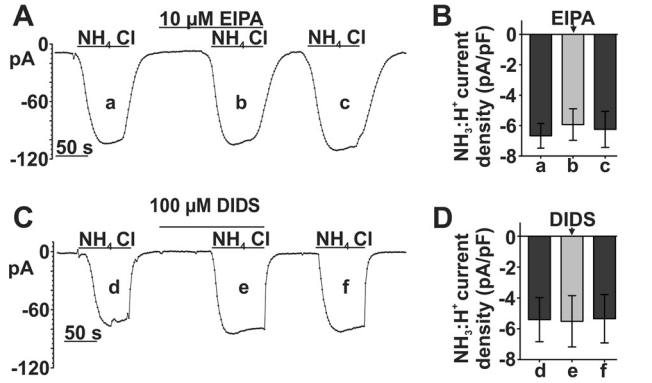

FIGURE 10. **SLC4A11 eNH$_4$Cl-dependent currents are inhibited by neither 10 μM EIPA nor 100 μM DIDS.** *A*, sample whole-cell current recording of eNH$_4$Cl-dependent current in SLC4A11 cells before (*a*), during (*b*), and after (*c*) 10 μM EIPA application. *B*, bar graph summary of eNH$_4$Cl-dependent current density before (*a*), during (*b*), and after (*c*) EIPA application ($n = 6$) (repeated measure ANOVA, $p = 0.298$). *C*, representative whole-cell current recording of eNH$_4$Cl-dependent current in SLC4A11 cells before (*d*), during (*e*), and after (*f*) 100 μM DIDS application. *D*, bar graph summary of eNH$_4$Cl-dependent current density before (*d*), during (*e*), and after (*f*) DIDS application ($n = 7$) (repeated measure ANOVA, $p = 0.847$). *Error bars*, S.E.

ability (9). In addition, it has been reported that DIDS has no effect on SLC4A11 Na^+-H^+ permeability (10), whereas another group reported that DIDS enhances SLC4A11 H^+ permeability (12). Therefore, we tested whether these two compounds affect the SLC4A11 NH_3/H^+ current in our model system. However, we found that neither 100 μM DIDS nor 10 μM EIPA affected NH_3/H^+ inward currents in SLC4A11-PS120 cells (Fig. 10). It is well known that DIDS is a broad spectrum inhibitor of anion transporters, whereas EIPA is a potent Na^+/H^+ exchanger inhibitor. These data suggest unique pharmacological properties for SLC4A11 expressed in NHE-deficient PS120 cells and indicate that the previous studies may be complicated by the presence of endogenous transporters influenced by SLC4A11 activity.

Discussion

In this study, we examined the potential mechanism for apparent NH_4^+ permeability of SLC4A11 (9). Using the NHE-deficient PS120 fibroblast cell line, we found evidence indicating that human SLC4A11 is an electrogenic NH_3/H^+ transporter. As such, SLC4A11 should be considered when examining ammonia: H^+ balance along with other recently identified NH_3 channels/transporters, namely selected AQPs (AQP8, AQP3, AQP7, AQP9, and AQP10) (14), Amt proteins, methylamine permease (22), and rhesus protein (23). In addition, our findings may also provide insight into the pathophysiology of corneal endothelial dystrophy (24, 25) and an explanation for altered renal function in SLC4A11 knock-out mice (7, 8).

We initially observed apparent SLC4A11 NH_4^+ permeability during studies of acid load recovery using an ammonium pulse approach. Significant acidification during the ammonium pulse was only seen in SLC4A11-PS120 cells. When Boron *et al.* (17) first studied NH_3-induced intracellular pH transients in the squid giant axon, it was calculated that the intracellular acidification during NH_4Cl pulse was due to a finite permeability to NH_4^+, and the acidification rate is determined mainly by the absolute NH_4^+ permeability. Also, the extent of the acid loading effect in the wash phase positively correlates with NH_4^+ permeability (17). Our data show that SLC4A11 transfection increased the apparent NH_4^+ permeability in PS120 cells relative to the low endogenous level in EV. SLC4A11 high expression Col4 and low expression Col12 showed higher and lower acidification rates, indicating that the apparent NH_4^+ (or NH_3-H^+ as equivalent) permeability is directly associated with SLC4A11 expression level.

The electrophysiological recordings revealed that SLC4A11-induced NH_4^+ (or NH_3-H^+) permeability results in NH_4Cl-dependent currents. The inward currents vary directly with solution $[NH_3]$ but not $[NH_4^+]$ and were relatively unaffected by removal of Na^+, K^+, or Cl^-. This is very similar to that observed in AQP8, which was proposed to be permeable to NH_3 rather than NH_4^+ due to the hydrophobic pore inside the channel (14, 23). Interestingly, there is evidence that SLC4A11 has water channel properties and shares one NP*X* motif with AQPs (13). NH_3 and H_2O share similar size and dipole moment (1.5 *versus* 1.8 debye), and the aromatic/arginine regions in AQPs provide selectivity of NH_3 over H_2O (15). In the current study, we observed an 84-fold increase in current in response to a 75-fold increase in $[NH_3]_o$ (Fig. 2), and when $[NH_3]$ is equalized in different pH solutions by adding more NH_4Cl at lower pH and less at high pH (Fig. 3), we observed similar current amplitude, strongly supporting NH_3 as the actual species transported. Furthermore, the ammonia analog MA has a similar molecular radius as NH_3 (26) but a significantly higher pK_a. So there is less free uncharged [MA] than $[NH_3]$ at the same pH, and as a result, MA generated less current in SLC4A11 than NH_3.

A distinctive characteristic of SLC4A11 that we observed here, which differentiates SLC4A11 from other ammonia channels/transporters, is that NH_3 is evidently co-transported with H^+. Unlike the ammonia- and H^+-permeable AQP1 Arg-195 mutant that shows H^+ currents in the absence of NH_3 (15), SLC4A11 shows no currents in response to proton gradient changes alone (Fig. 5*A*). Proton gradient changes can induce currents only after NH_4Cl pulse (Fig. 2, *filled arrow*, and Fig. 5, *B* and *D*). When equalizing $[NH_3]_o$ (Fig. 3), extracellular pH or $[H^+]$ gradient differences can affect apparent kinetics and current density of eNH$_4$Cl-dependent current. Reversal potential analysis of currents during and after NH_4Cl pulse is also consistent with an NH_3/H^+ co-transport hypothesis. Although H^+ is the putative charge carrier in the currents of all electrogenic NH_3 channels/transporters, we show here, for the first time, evidence that H^+ is co-transported with NH_3 in SLC4A11. A coupled transport of H^+ and NH_3 may be more beneficial for the cell because it would produce smaller cytosolic pH_i transients than if NH_3 were transported alone.

As an $NH_3/2H^+$ co-transporter, the direction of SLC4A11 transport depends on the $[NH_3]$ gradient, $[H^+]$ gradient, and cell membrane potential. In most of the experiments, the holding potential was -60 mV, and we introduced an inward $[NH_3]$ gradient that resulted in inward currents. However, we observed outward currents on multiple occasions: 1) during pH 8.5 wash after pH 8.5 NH_4Cl (Fig. 5*C*, time *c*); 2) prominent and prolonged outward currents during wash periods in cells dialyzed with NH_4Cl (Fig. 7*A*); 3) smaller outward currents

observed during pH 8.5 wash following pH 7.5 eNH_4Cl (Fig. 5*B*); 4) outward break-in currents observed with I1-NH_4Cl dialysis if the holding potential was reduced to −10 mV (Fig. 7, *D* and *E*); 5) at −10 mV with I1-NH_4Cl dialysis, outward currents were observed in pH 7.5 wash after pH 7.5 NH_4Cl (Fig. 7*D*). Given a 1:2 NH_3/H^+ stoichiometry of SLC4A11 at pH_o 7.5, in a typical cell with pH_i 7.1 and membrane potential of −50 mV, an ~15-fold $[NH_3]$ outward gradient is needed to drive SLC4A11 transport in the outward direction. This could potentially be achieved, for example, in glutamine-metabolizing cells that generate significant amounts of NH_3 (27, 28). Although NH_3 can diffuse across most cell membranes, a NH_3/H^+ co-transporter like SLC4A11 may offer an advantage of directional regulated ammonia transport, which could play an important role in the function of ammonia detoxification like other ammonia channels (*e.g.* AQP8 (27)).

Although the net movement of NH_3/H^+ is physiologically equivalent to NH_4^+, transport of NH_3 over NH_4^+ offers the advantage of high selectively. K^+ and NH_4^+ ions are similar in several characteristics that are important for membrane transport: 1) they share an almost identical radius (NH_4^+ 0.148 nm *versus* K^+ 0.141 nm) (29); 2) they have similar charge (15); and 3) hydration energies are also similar (30). Therefore, it is not surprising that multiple K^+ transporters/channels allow substitution of NH_4^+ for K^+ (*e.g.* in the Na-K-2Cl co-transporter NKCC2 and barium-sensitive K^+ channels (31)). Reverse substitution could possibly occur in NH_4^+-selective transporters to carry K^+ nonspecifically (15). To avoid this, the Amt NH_4^+ channel uses a two-step translocation process involving a hydrophobic pore to discriminate NH_4^+ from K^+ (32). For SLC4A11, transport of NH_3 instead of NH_4^+ may also help resolve the selectivity problem. Because K^+ free extracellular and intracellular solutions were used in most of the experiments presented here, K^+ involvement in the recorded currents is unlikely. Indeed, K^+ is not a substrate for SLC4A11 shown in Fig. 4*A* comparing current density in 5 mM K^+ E1 *versus* K^+ free E4. This suggests that SLC4A11 utilizes a mechanism ensuring its relative selectivity. However, greater understanding of the molecular mechanisms underlying the processes would require further investigation.

Park *et al.* (10) reported increased baseline pH_i in SLC4A11-transfected HEK293 cells, whereas our previous study reported no difference (9). Consistent with a more recent report (12), here we observed reduced baseline pH_i in SLC4A11-PS120 cells (Fig. 6*A*). Although the H^+ permeability is evident, in the absence of NH_3, the H^+ fluxes are very small, and no measureable H^+ current can be recorded. Interestingly, the effect on baseline pH_i is made most evident in PS120 cells because of the lack of Na^+/H^+ exchangers. Previous studies show that when a more robust bicarbonate buffering system is present, baseline pH_i differences disappear (9, 10, 12). This suggests that SLC4A11 H^+ permeability in the absence of ammonia is a relatively small contributor to pH_i regulation, whereas ammonia transport through SLC4A11 is of more physiological relevance.

Park *at al.* (10) also concluded that SLC4A11 is an Na^+-coupled borate transporter (with a capability to transport hydroxyl ions (OH^-) in the absence of borate). Interestingly, boric acid is a weak acid with a pK_a of 9.24, which is very close to that of NH_3 (pK_a = 9.25), making it largely exist as uncharged H_3BO_3 at physiological pH (33). The structure of boric acid is comparable with that of NH_3, with the central boron atom possessing three valence electrons, as nitrogen does in NH_3. The molecular radius of boric acid (2.573 Å) is comparable with that of urea (2.618 Å), which is also permeable through some ammonia-permeable AQPs (14). If a hydrophobic environment does exist in SLC4A11 supporting NH_3 transport, it may provide a path for the uncharged boric acid.

This study has several limitations. Because of the ability of Na^+ to modulate SLC4A11 activity at pH 8.5, we only determined the apparent stoichiometry of NH_3/H^+ transport at the physiological pH 7.5, under which Na^+ does not appear to have any effect on eNH_4Cl-dependent currents. We are also aware of the limitation of sequential NH_4Cl superfusion during which the assumption of constant $[NH_3]_i$ and $[H^+]_i$ is uncertain. Indeed, there was current inhibition at high NH_4Cl concentrations, possibly due to increased $[NH_3]_i$, which could lead to an underestimation of E_{rev}. Notably, plotting the plateau E_{rev} data *versus* $\log[NH_3]_o$ yielded a smaller slope, however still closest to the 1:2 NH_3/H^+ model. Also, because NH_3 is diffusible through the PS120 cell membrane (shown in Fig. 1), we are not able to control $[NH_3]_i$ and $[H^+]_i$ more tightly. In addition, the possibility of NH_4^+-H^+-coupled transport cannot be completely eliminated. Therefore, future investigations, such as SLC4A11 protein reconstitution into a planar lipid bilayer or SLC4A11 expression in an NH_3-impermeable cell line, would be useful to clarify the uncertainties with the 1:2 NH_3/H^+ model.

In healthy individuals, urine ammonia concentration is around 30–50 mM, whereas plasma ammonia concentration ranges between 0.005 and 0.02 mM. Plasma ammonia can rise to 0.1 mM under pathophysiological conditions. The fact that we were able to record currents from 1 to 100 mM eNH_4Cl (0.0017–17 mM (NH_3)) with no saturation indicates that SLC4A11 can efficiently function in the physiological ammonia range. Ammonia channels/transporters play important roles in nitrogen homeostasis, not only in the major nitrogen handling organs like liver and kidney (27, 34), but also in lung (35), male reproductive system (36), and gastrointestinal tract (37). Directional ammonia transport capacity offered by SLC4A11 can play essential roles in ammonia detoxification in a wide range of tissues/cells. Especially in cells that actively metabolize glutamine and glutamate, such as neurons, skeletal muscle cells, and gastrointestinal tract epithelium (38, 39), ammonia is a major waste product that needs to be extruded. Indeed, SLC4A11 is not only associated with corneal endothelial dystrophy, but also may play roles in other physiological and pathophysiology processes. The ubiquitous expression of SLC4A11, in cornea endothelium, kidney, inner ear, salivary glands (submandibular and parotid), thyroid, mammary gland, testis, trachea, esophagus, pancreas, liver, spleen, and cerebellum (1, 6, 10) suggests a diverse physiological role. Because SLC4A11 is highly expressed in cornea endothelium, fibrocytes of the inner ear, and the loop of Henle, these three tissues could be the starting point for investigating SLC4A11 physiological function in regulating tissue nitrogen levels. It is well known that cornea and inner ear function depends on tightly controlled fluid and ion transport. At least 60 mutations have been identified as being associated

with corneal endothelial dystrophy and/or perceptive deafness (40). A recent clinical study suggests that homozygous SLC4A11 mutated congenital hereditary endothelial dystrophy patients progress to Harboyan syndrome at a later age (perceptive deafness and corneal endothelial dystrophy (41)), whereas another study associated SLC4A11 mutants with the corneal ectasia disorder keratoconus (42). In the kidney, SLC4A11 is highly expressed in the thin descending limb of loop of Henle (7). Henle's loop epithelium has the capacity to reabsorb ammonia into interstitial spaces and, through the countercurrent multiplication mechanism, create a cortical-medullary increasing ammonium gradient to regulate urine ammonium excretion (18). In SLC4A11 knock-out mice, an impairment in the countercurrent multiplication process was suggested based on polyuria and urine hypo-osmolality (7). The ammonia transport property of SLC4A11 suggests that it can potentially play a role in medullary interstitial ammonia handling and ammonia countercurrent multiplication (18, 31), filling the missing piece of renal ammonia transport (31).

In summary, we have identified SLC4A11 as an additional member of the subfamily of ammonia channels and transporters and as an H^+-coupled ammonia transporter with an apparent stoichiometry of 1:2 NH_3/H^+. The SLC4A11 ammonia current is independent of K^+, Na^+, and Cl^- at physiological pH and is uniquely insensitive to DIDS and EIPA. These findings provide mechanistic insights into the physiological and pathophysiological processes that may occur in the cornea, kidney, and inner ear.

Author Contributions—W. Z., J. A. B., and A. G. O. conceived and coordinated the study and wrote the paper. W. Z., D. G. O., and J. A. B. designed and W. Z. and D. G. O. performed and analyzed the experiments shown in Figs. 1 and 6. W. Z., J. A. B., and A. G. O. designed and W. Z. performed and analyzed the electrophysiological experiments shown in Figs. 2–5 and 7–10. All authors reviewed the results and approved the final version of the manuscript.

Acknowledgment—We thank Dr. Eranga Vithana (Singapore Eye Research Institute) for the SLC4A11-HA plasmid.

References

1. Parker, M. D., Ourmozdi, E. P., and Tanner, M. J. A. (2001) Human BTR1, a new bicarbonate transporter superfamily member and human AE4 from kidney. *Biochem. Biophys. Res. Commun.* **282,** 1103–1109
2. Damkier, H. H., Nielsen, S., and Praetorius, J. (2007) Molecular expression of SLC4-derived Na^+-dependent anion transporters in selected human tissues. *Am. J. Physiol. Regul. Integr. Comp. Physiol.* **293,** R2136–R2146
3. Shei, W., Liu, J., Htoon, H. M., Aung, T., and Vithana, E. N. (2013) Differential expression of the Slc4 bicarbonate transporter family in murine corneal endothelium and cell culture. *Mol. Vision* **19,** 1096–1106
4. Aldave, A. J., Han, J., and Frausto, R. F. (2013) Genetics of the corneal endothelial dystrophies: an evidence-based review. *Clin. Genet.* **84,** 109–119
5. Gottsch, J. D., Bowers, A. L., Margulies, E. H., Seitzman, G. D., Kim, S. W., Saha, S., Jun, A. S., Stark, W. J., and Liu, S. H. (2003) Serial analysis of gene expression in the corneal endothelium of Fuchs' dystrophy. *Invest. Ophthalmol. Vis. Sci.* **44,** 594–599
6. Lopez, I. A., Rosenblatt, M. I., Kim, C., Galbraith, G. C., Jones, S. M., Kao, L., Newman, D., Liu, W., Yeh, S., Pushkin, A., Abuladze, N., and Kurtz, I. (2009) Slc4a11 gene disruption in mice: cellular targets of sensorineuronal abnormalities. *J. Biol. Chem.* **284,** 26882–26896
7. Gröger, N., Fröhlich, H., Maier, H., Olbrich, A., Kostin, S., Braun, T., and Boettger, T. (2010) SLC4A11 prevents osmotic imbalance leading to corneal endothelial dystrophy, deafness, and polyuria. *J. Biol. Chem.* **285,** 14467–14474
8. Han, S. B., Ang, H. P., Poh, R., Chaurasia, S. S., Peh, G., Liu, J., Tan, D. T., Vithana, E. N., and Mehta, J. S. (2013) Mice with a targeted disruption of Slc4a11 model the progressive corneal changes of congenital hereditary endothelial dystrophy. *Invest. Ophthalmol. Vis. Sci.* **54,** 6179–6189
9. Ogando, D. G., Jalimarada, S. S., Zhang, W., Vithana, E. N., and Bonanno, J. A. (2013) SLC4A11 is an EIPA-sensitive Na^+-permeable pH_i regulator. *Am. J. Physiol. Cell Physiol.* **305,** C716–C727
10. Park, M., Li, Q., Shcheynikov, N., Zeng, W., and Muallem, S. (2004) NaBC1 is a ubiquitous electrogenic Na^+-coupled borate transporter essential for cellular boron homeostasis and cell growth and proliferation. *Mol. Cell* **16,** 331–341
11. Jalimarada, S. S., Ogando, D. G., Vithana, E. N., and Bonanno, J. A. (2013) Ion transport function of SLC4A11 in corneal endothelium. *Invest. Ophthalmol. Vis. Sci.* **54,** 4330–4340
12. Kao, L., Azimov, R., Abuladze, N., Newman, D., and Kurtz, I. (2015) Human SLC4A11-C functions as a DIDS-stimulatable $H^+(OH^-)$ permeation pathway: partial correction of R109H mutant transport. *Am. J. Physiol. Cell Physiol.* **308,** C176–C188
13. Vilas, G. L., Loganathan, S. K., Liu, J., Riau, A. K., Young, J. D., Mehta, J. S., Vithana, E. N., and Casey, J. R. (2013) Transmembrane water-flux through SLC4A11: a route defective in genetic corneal diseases. *Hum. Mol. Genet.* **22,** 4579–4590
14. Litman, T., Søgaard, R., and Zeuthen, T. (2009) in *Aquaporins* (Beitz, E., ed) pp. 327–358, Springer, Berlin
15. Beitz, E., Wu, B., Holm, L. M., Schultz, J. E., and Zeuthen, T. (2006) Point mutations in the aromatic/arginine region in aquaporin 1 allow passage of urea, glycerol, ammonia, and protons. *Proc. Natl. Acad. Sci. U.S.A.* **103,** 269–274
16. Thomas, J. A., Buchsbaum, R. N., Zimniak, A., and Racker, E. (1979) Intracellular pH measurements in Ehrlich ascites tumor cells utilizing spectroscopic probes generated *in situ*. *Biochemistry* **18,** 2210–2218
17. Boron, W. F., and De Weer, P. (1976) Intracellular pH transients in squid giant axons caused by CO_2, NH_3, and metabolic inhibitors. *J. Gen. Physiol.* **67,** 91–112
18. Packer, R. K., Desai, S. S., Hornbuckle, K., and Knepper, M. A. (1991) Role of countercurrent multiplication in renal ammonium handling: regulation of medullary ammonium accumulation. *J. Am. Soc. Nephrol.* **2,** 77–83
19. Yao, H., Ma, E., Gu, X.-Q., and Haddad, G. G. (1999) Intracellular pH regulation of CA1 neurons in Na^+/H^+ isoform 1 mutant mice. *J. Clin. Invest.* **104,** 637–645
20. Nakhoul, N. L., Abdulnour-Nakhoul, S. M., Boulpaep, E. L., Rabon, E., Schmidt, E., and Hamm, L. L. (2010) Substrate specificity of Rhbg: ammonium and methyl ammonium transport. *Am. J. Physiol. Cell Physiol.* **299,** C695–C705
21. Virkki, L. V., Wilson, D. A., Vaughan-Jones, R. D., and Boron, W. F. (2002) Functional characterization of human NBC4 as an electrogenic Na^+-HCO cotransporter (NBCe2). *Am. J. Physiol. Cell Physiol.* **282,** C1278–C1289
22. Winkler, F. K. (2006) Amt/MEP/Rh proteins conduct ammonia. *Pflugers Arch.* **451,** 701–707
23. Nakhoul, N. L., Abdulnour-Nakhoul, S. M., Schmidt, E., Doetjes, R., Rabon, E., and Hamm, L. L. (2010) pH sensitivity of ammonium transport by Rhbg. *Am. J. Physiol. Cell Physiol.* **299,** C1386–C1397
24. Ramprasad, V. L., Ebenezer, N. D., Aung, T., Rajagopal, R., Yong, V. H., Tuft, S. J., Viswanathan, D., El-Ashry, M. F., Liskova, P., Tan, D. T., Bhattacharya, S. S., Kumaramanickavel, G., and Vithana, E. N. (2007) Novel SLC4A11 mutations in patients with recessive congenital hereditary endothelial dystrophy (CHED2). Mutation in brief #958. Online. *Hum. Mutat.* **28,** 522–523
25. Vithana, E. N., Morgan, P. E., Ramprasad, V., Tan, D. T., Yong, V. H., Venkataraman, D., Venkatraman, A., Yam, G. H., Nagasamy, S., Law, R. W., Rajagopal, R., Pang, C. P., Kumaramanickevel, G., Casey, J. R., and Aung, T. (2008) SLC4A11 mutations in Fuchs endothelial corneal dystrophy. *Hum. Mol. Genet.* **17,** 656–666

26. Cohen, B. N., Labarca, C., Davidson, N., and Lester, H. A. (1992) Mutations in M2 alter the selectivity of the mouse nicotinic acetylcholine receptor for organic and alkali metal cations. *J. Gen. Physiol.* **100,** 373–400
27. Soria, L. R., Marrone, J., Calamita, G., and Marinelli, R. A. (2013) Ammonia detoxification via ureagenesis in rat hepatocytes involves mitochondrial aquaporin-8 channels. *Hepatology* **57,** 2061–2071
28. Albrecht, J., and Norenberg, M. D. (2006) Glutamine: a Trojan horse in ammonia neurotoxicity. *Hepatology* **44,** 788–794
29. Lima, A. S., Bocchi, N., Gomes, H. M., and Teixeira, M. F. (2009) An electrochemical sensor based on nanostructured hollandite-type manganese oxide for detection of potassium ions. *Sensors* **9,** 6613–6625
30. ten Hoopen, F., Cuin, T. A., Pedas, P., Hegelund, J. N., Shabala, S., Schjoerring, J. K., and Jahn, T. P. (2010) Competition between uptake of ammonium and potassium in barley and *Arabidopsis* roots: molecular mechanisms and physiological consequences. *J. Exp. Bot.* **61,** 2303–2315
31. Houillier, P., and Bourgeois, S. (2012) More actors in ammonia absorption by the thick ascending limb. *Am. J. Physiol. Renal Physiol.* **302,** F293–F297
32. Khademi, S., O'Connell, J., 3rd, Remis, J., Robles-Colmenares, Y., Miercke, L. J., and Stroud, R. M. (2004) Mechanism of ammonia transport by Amt/MEP/Rh: structure of AmtB at 1.35 Å. *Science* **305,** 1587–1594
33. Tanaka, M., Wallace, I. S., Takano, J., Roberts, D. M., and Fujiwara, T. (2008) NIP6;1 is a boric acid channel for preferential transport of boron to growing shoot tissues in *Arabidopsis*. *Plant Cell* **20,** 2860–2875
34. Weiner, I. D., and Verlander, J. W. (2010) Molecular physiology of the Rh ammonia transport proteins. *Curr. Opin. Nephrol. Hypertens.* **19,** 471–477
35. Han, K. H., Mekala, K., Babida, V., Kim, H. Y., Handlogten, M. E., Verlander, J. W., and Weiner, I. D. (2009) Expression of the gas-transporting proteins, Rh B glycoprotein and Rh C glycoprotein, in the murine lung. *Am. J. Physiol. Lung Cell. Mol. Physiol.* **297,** L153–L163
36. Lee, H. W., Verlander, J. W., Handlogten, M. E., Han, K. H., Cooke, P. S., and Weiner, I. D. (2013) Expression of the rhesus glycoproteins, ammonia transporter family members, RHCG and RHBG in male reproductive organs. *Reproduction* **146,** 283–296
37. Handlogten, M. E., Hong, S. P., Zhang, L., Vander, A. W., Steinbaum, M. L., Campbell-Thompson, M., and Weiner, I. D. (2005) Expression of the ammonia transporter proteins Rh B glycoprotein and Rh C glycoprotein in the intestinal tract. *Am. J. Physiol. Gastrointest. Liver Physiol.* **288,** G1036–G1047
38. Newsholme, P., Lima, M. M., Procopio, J., Pithon-Curi, T. C., Doi, S. Q., Bazotte, R. B., and Curi, R. (2003) Glutamine and glutamate as vital metabolites. *Braz. J. Med. Biol. Res.* **36,** 153–163
39. Newsholme, P., Procopio, J., Lima, M. M., Pithon-Curi, T. C., and Curi, R. (2003) Glutamine and glutamate: their central role in cell metabolism and function. *Cell Biochem. Funct.* **21,** 1–9
40. Vilas, G. L., Morgan, P. E., Loganathan, S. K., Quon, A., and Casey, J. R. (2011) A biochemical framework for SLC4A11, the plasma membrane protein defective in corneal dystrophies. *Biochemistry* **50,** 2157–2169
41. Siddiqui, S., Zenteno, J. C., Rice, A., Chacón-Camacho, O., Naylor, S. G., Rivera-de la Parra, D., Spokes, D. M., James, N., Toomes, C., Inglehearn, C. F., and Ali, M. (2014) Congenital hereditary endothelial dystrophy caused by SLC4A11 mutations progresses to Harboyan syndrome. *Cornea* **33,** 247–251
42. Nowak, D. M., Karolak, J. A., Kubiak, J., Gut, M., Pitarque, J. A., Molinari, A., Bejjani, B. A., and Gajecka, M. (2013) Substitution at IL1RN and deletion at SLC4A11 segregating with phenotype in familial keratoconus. *Invest. Ophthalmol. Vis. Sci.* **54,** 2207–2215